Electronic Supplementary Material (ESI) for Dalton Transactions.
This journal is © The Royal Society of Chemistry 2024

Investigation of the spin crossover behaviour of a sublimable Fe(II)-qsal complex: from the bulk to a submonolayer on graphene/SiO_2

Adelais Trapali, [a] Mukil Muppal, [b] Satakshi Pandey, [c] Marie-Laure Boillot, [a] Vincent Repain, [b] Yannick. J. Dappe, [d] Jean-François Dayen, [c] Eric Rivière, [a] Régis Guillot, [a] Marie-Anne Arrio, [e] Edwige Otero, [f] Amandine Bellec, *[b] and Talal Mallah *[a]

Synthesis of Hqsal-NEt_2.[1] 8-aminoquinoline (649 mg, 4.5 mmol, 0.9 eq.) was added to a stirring solution of 4-(diethylamino)salicylaldehyde (966 mg, 5 mmol, 1.0 eq.) in MeOH (75 mL). The reaction mixture was stirred for 2 h at room temperature and then refluxed for 56 h. The progress of the reaction was monitored with thin-layer chromatography (TLC, Ethyl acetate). Once the reaction was completed, the solution was cooled to room temperature and evaporated until dryness, affording an orange-brown oil residue. Hqsal-$5NEt_2$ was obtained as a brown solid after its purification via column chromatography (SiO_2, Ethyl acetate). Yield: 49.3 %. ^{1}H NMR (400 MHz, DMSO-d_6): δ 14.68 (d, J= 4.12 Hz, 1H), 8.95 (dd, J_1= 4.12 Hz, J_2= 1.72 Hz, 1H), 8.78 (d, J= 4.12 Hz, 1H), 8.39 (dd, J_1= 8.32 Hz, J_2= 1.68 Hz, 1H), 7.76 (m, 2H), 7.62 (m, 2H), 7.28 (d, J= 9.0 Hz, 1H), 6.30 (dd, J_1= 9.00 Hz, J_2= 2.4 Hz, 1H), 5.92 (d, J= 2.4 Hz, 1H), 3.40 (q, J= 7.0 Hz, 4H), 1.14 (t, J= 7.0 Hz, 6H) ppm. ^{13}C NMR (100.6 MHz, DMSO-d_6): δ 169.0, 157.8, 152.5, 150.0, 142.6, 140.9, 136.2, 134.6, 128.7, 126.9, 124.3, 122.0, 115.8, 109.6, 104.5, 97.4, 43.6, 12.7 ppm. ESI: calc. m/z = 320.1757 [M+1] for chemical formula $C_{20}H_{22}N_3O$, found 320.1749.

a)

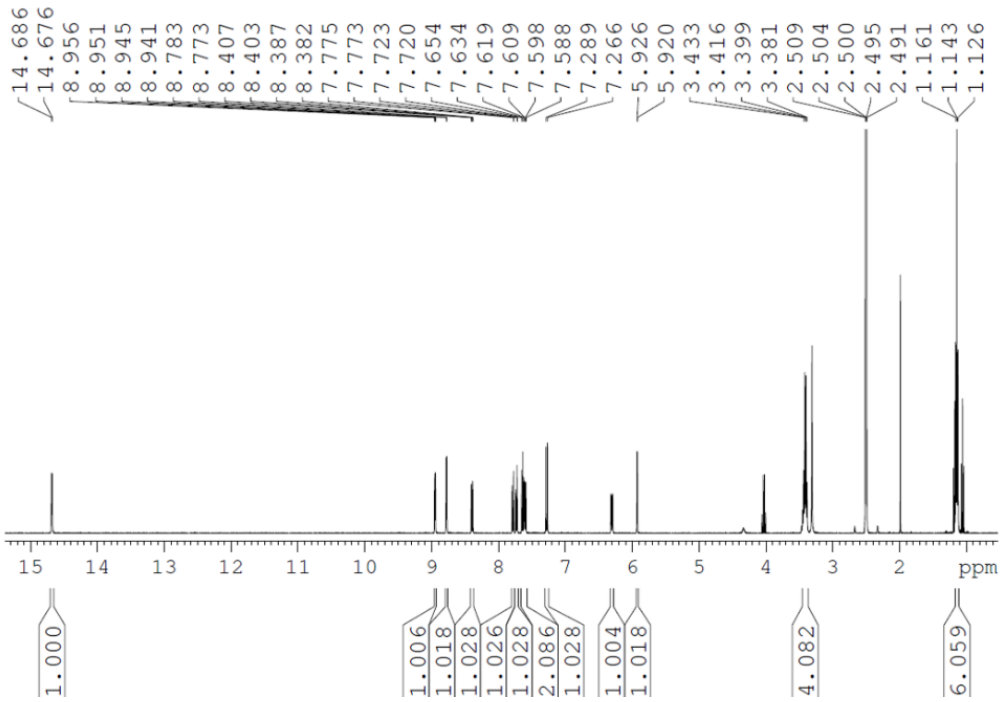

[1] Y. Li, J. Wu, X. Jin, J. Wang, S. Han, W. Wu, J. Xu, W. Liu, X. Yao and Y. Tang, *Dalton Trans.*, 2014, **43(**4), 1881-1887

b)

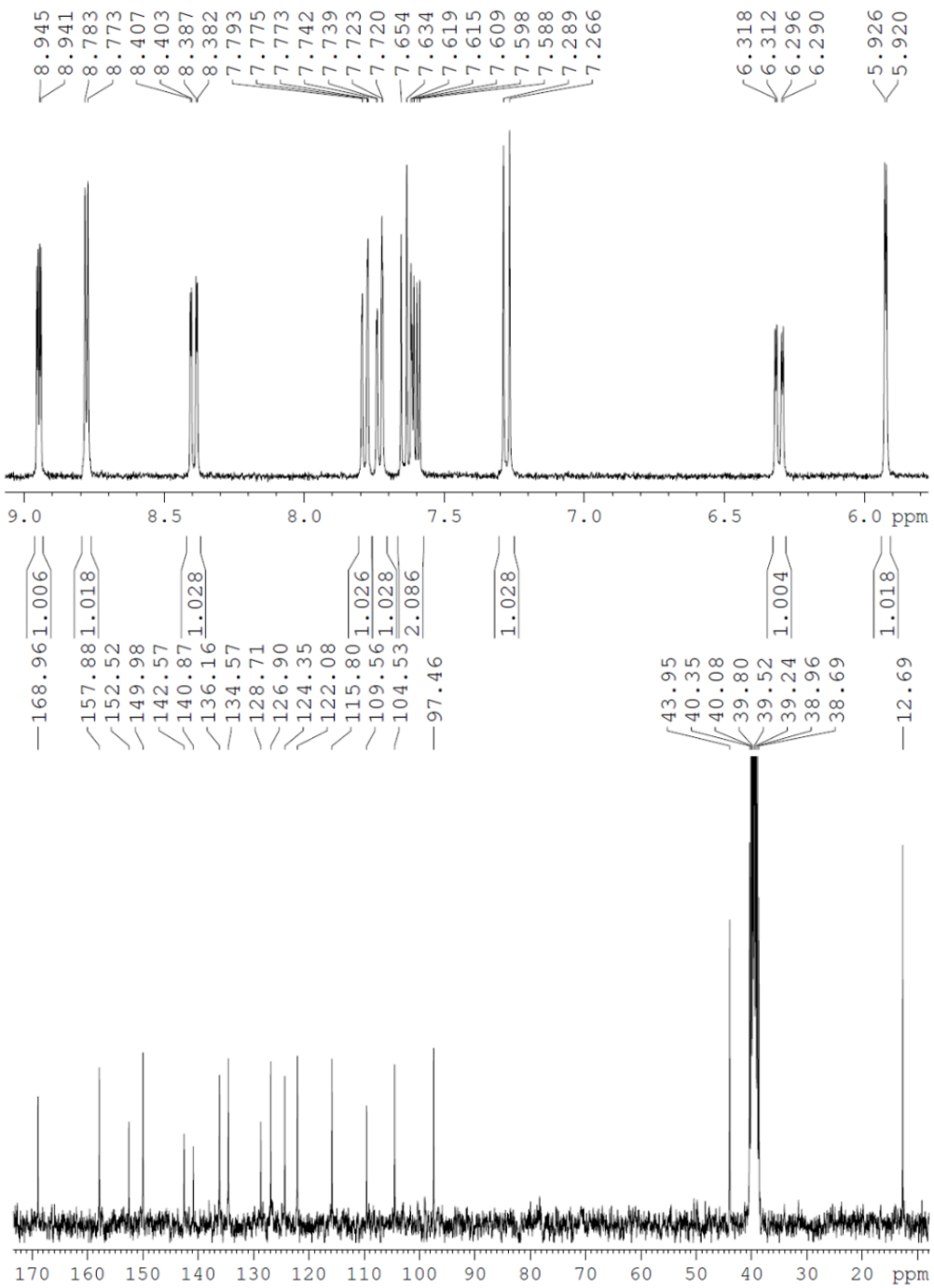

c)

Figure S1. ^{1}H NMR of Hqsal-NEt_2 recorded at room temperature (400 MHz, DMSO-d_6) (a), zoom on the aromatic region of the ^{1}H NMR (b) and ^{13}C NMR of Hqsal-NEt_2 recorded at room temperature (100.6 MHz, DMSO-d_6) (c)

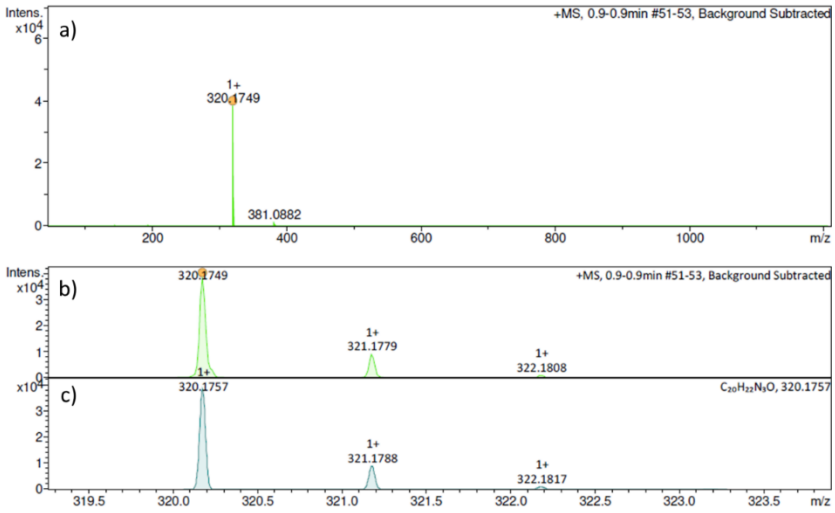

Figure S2. ESI-MS spectrum of Hqsal-NEt_2 (a) with its experimental (b) and simulated (c) isotopic pattern.

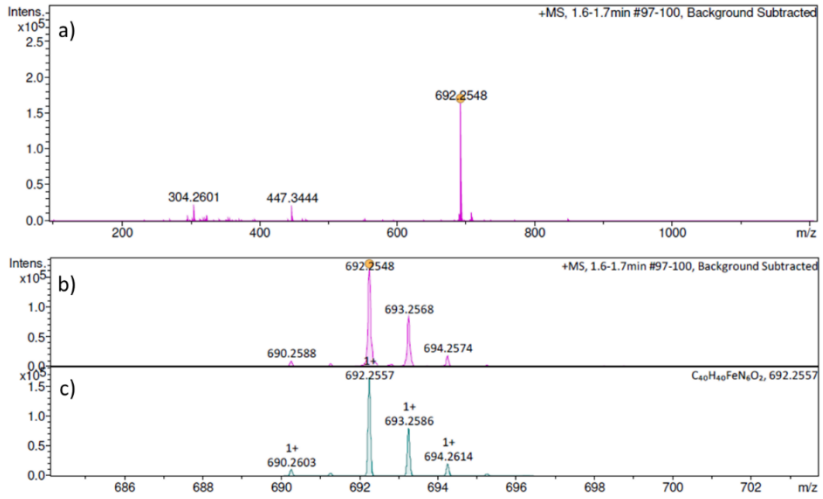

Figure S3. ESI-MS spectrum of Fe(qsal-NEt_2)$_2$ (a), a zoom of the experimental (b) and simulated isotopic pattern (c).

Synthesis of [Feqsal-NEt_2]Cl: $FeCl_3$ (10.1 mg, 0.0625 mmol, 1.0 eq.) was dissolved in MeOH (4 mL), and the resulting solution was carefully layered on top of a dichloromethane solution (4 mL) of Hqsal-NEt_2 (40 mg, 0.125 mmol, 2.0 eq.) containing 2.08 eq. of Et_3N. After 5 days of standing under ambient conditions, [Feqsal-NEt_2]Cl precipitated as a black solid, collected via filtration, washed with MeOH (3 x 0. 5 mL) and dichloromethane (3 x 0. 5 mL), and dried under vacuum. Yield: 85 %. ESI: calc. m/z = 692.2557 $[Feqsal\text{-}NEt_2]^+$ for chemical formula $[C_{40}H_{40}FeN_6O_2]$, found 692.2562.

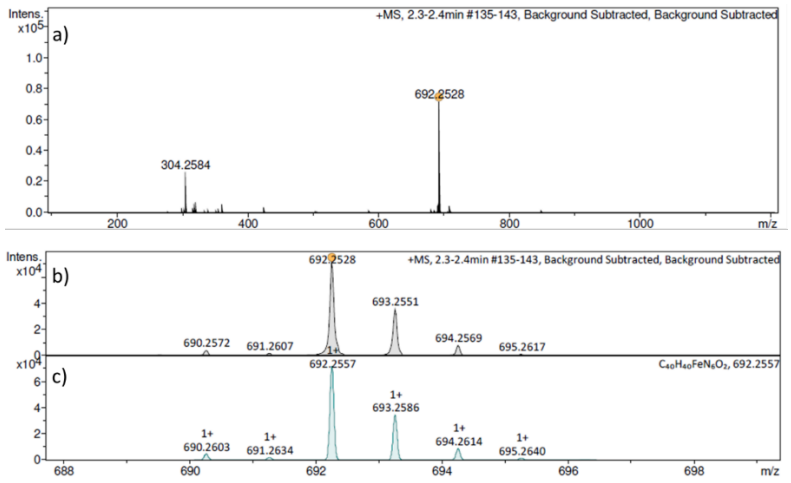

Figure S4. ESI-MS spectrum of [Fe(qsal-NEt_2)$_2$]Cl (a) a zoom of the experimental (b) and simulated isotopic pattern (c).

Single Crystal X-ray diffraction data.

The structures were solved by direct methods using SHELXS-97[2] and refined against F^2 by full-matrix least-squares techniques using SHELXL-2018[3] with anisotropic displacement parameters for all non-hydrogen atoms. All calculations were performed by using the Crystal Structure crystallographic software package WINGX.[4]

The crystal data collection and refinement parameters are given in Table S1.

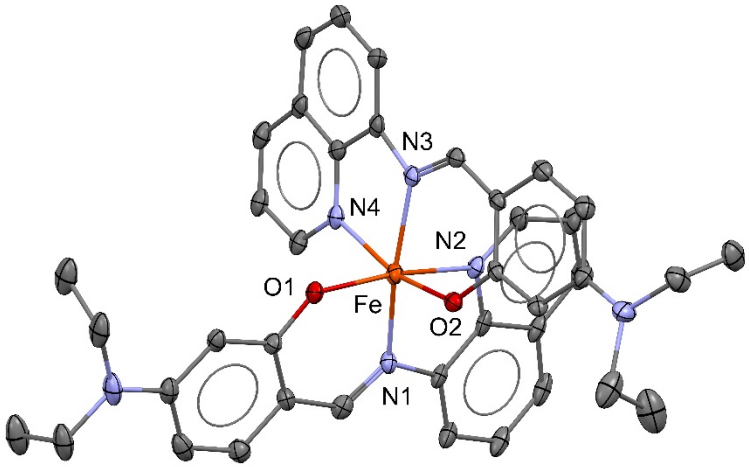

Figure S5. An ORTEP drawing of the complex [Fe(qsal-NEt_2)$_2$]. Thermal ellipsoids are shown at the 10% level (*hydrogen* atoms and solvent are omitted for clarity).

[2] G. M. Sheldrick, SHELXS-97, Program for Crystal Structure Solution, University of Göttingen, Göttingen, Germany, **1997**.
[3] G. M. Sheldrick, *Acta Crystallogr., Sect. A: Found. Crystallogr.,* **2008**, *64*, 112-122.
[4] L. J. Farrugia, *J. Appl. Cryst*. **1999**, *32*, 837.

Table S1. Crystallographic data and structure refinement details.

Compound	**Fe(qsal-NEt$_2$)$_2$**	
T, K	90(1)	200(1)
CCDC	2350748	2350749
Empirical Formula	C_{40} H_{40} Fe N_6 O_2, 3/2 (C H_4 O)	C_{40} H_{40} Fe N_6 O_2, C H_4 O
M_r (g/mol)	740.69	720.64
Crystal size, mm^3	0.06 x 0.04 x 0.01	0.07 x 0.03 x 0.01
Crystal system	monoclinic	monoclinic
Space group	*P* 2$_1$/*n*	*P* 2$_1$/*n*
a, Å	11.2330(14)	11.513(3)
b, Å	12.8503(18)	13.193(3)
c, Å	25.106(3)	23.640(6)
α, °	90	90
β, °	91.565(5)	96.376(7)
γ, °	90	90
Cell volume, Å^3	3622.7(8)	3568.4(15)
Z ; Z’	4 ; 1	4 ; 1
Radiation type ; wavelength Å	MoKα ; 0.71073	MoKα ; 0.71073
F_{000}	1564	1512
μ, mm^{-1}	0.467	0.471
range, °	1.967 - 26.393	2.065 - 23.341
Reflection collected	44 026	85 416
Reflections unique	7 289	5 158
R_{int}	0.1724	0.2802
GOF	1.010	1.016
Refl. obs. (*I*>2(*I*))	2 644	2 351
Parameters ; restraints	484 ; 6	464 ; 2
wR_2 (all data)	0.3161	0.2680
R value (*I*>2(*I*))	0.0992	0.0929
Largest diff. peak and hole (e-.Å^{-3})	0.631 ; -0.443	0.609 ; -0.398

Table S2. Selected bond lengths [Å] and angles [°] for compound Fe(qsal-NEt_2)$_2$ (cf. Figure S1. for the labels). All esds are estimated using the value of the full covariance matrix of least square. N_{im} and N_q are nitrogen atoms of the imine and the quinoline groups of the qsal-NEt_2, respectively.

T (K)	90	200
Fe-O1	1.911(5)	2.023(6)
Fe-O2	1.927(5)	2.013(6)
Fe-N1 (N_{im})	2.061(6)	2.123(8)
Fe-N2 (N_q)	2.188(5)	2.230(8)
Fe-N3 ($N_{im)}$	2.086(6)	2.132(8)
Fe-N4 (N_q)	2.170(7)	2.231(8)
O1-Fe-O2	95.6(2)	95.7(2)
O1-Fe-N1	91.4(2)	87.6(3)
O1-Fe-N2	166.8(2)	161.8(3)
O1-Fe-N3	101.1(2)	101.7(3)
O1-Fe-N4	88.4(2)	91.1(2)
O2-Fe-N1	97.9(2)	101.5(2)
O2-Fe-N2	91.8(2)	92.3(2)
O2-Fe-N3	88.3(2)	87.0(3)
O2-Fe-N4	165.3(3)	162.5(3)
N1-Fe-N2	76.8(2)	74.8(3)
N1-Fe-N3	165.5(2)	166.8(3)
N1-Fe-N4	96.1(3)	94.8(3)
N2-Fe-N3	89.9(2)	95.0(3)
N2-Fe-N4	87.1(2)	86.0(3)
N3-Fe-N4	77.0(3)	75.8(3)

Table S3. Comparison of the structural parameters of Fe(qsal-NEt_2)$_2$ with similar Fe(II) Schiff base complexes reported in the literature. N_{im} and N_q are the nitrogen atoms of the imine and the quinoline groups of the ligand, respectively. Fe-L refers to the average bond lengths. For Fe(qsal-NEt_2)$_2$, Σ and Θ parameters were calculated with OctaDist Software,[5] while for the rest of the complexes were recalculated using the same software for a more accurate comparison. Boxes highlight the complexes that undergo SCO. All distances are in Å.

	Spin State	T (K)	<Fe-N_{im}>	<Fe-N_q>	<Fe-O>	Fe-L	Σ	Θ	Ref.
Fe(qsal-COOH)$_2$·MeOH	HS	170	2.155	2.193	2.056	2.135	83.9206	308.4783	6
	LS	100	1.945	1.961	1.980	1.962	40.6822	113.0091	6
Fe(qsal-COOH)$_2$·MeOH ·H_2O	HS	170	2.180 2.178	2.228 2.237	2.076 2.073	2.161 2.163	72.8929 102.1311	279.2575 322.2542	6
		100	2.170 2.171	2.218 2.229	2.068 2.069	2.152 2.156	72.8163 101.9752	278.4097 320.9713	
Fe(qnal-12)$_2$·2C_6H_6	HS	120	2.131	2.218	2.027	2.125	84.2094	304.6750	7
Fe(qnal)$_2$·CH_2Cl_2	HS	293.1	2.140	2.189	2.015	2.114	83.6584	283.2334	8,9
	LS	123.1	1.934	1.953	1.942	1.943	33.8373	107.7173	8,9
Fe(qsal-Cl)$_2$	HS	348	2.122	2.166	2.004	2.096	72.0699	237.3975	10
	LS	100	1.932	1.950	1.958	1.946	32.5867	101.4254	10
Fe(qsal-F)$_2$	HS	100	2.177	2.191	2.023	2.130	86.8769	315.7932	10
Fe(qsal-Cl)$_2$	HS	330	2.113	2.158	2.009	2.093	69.1956	230.7959	11
	LS	100	1.938	1.953	1.957	1.949	33.8032	105.4724	11
Fe(qsal-Br)$_2$	HS	380	2.135	2.161	2.004	2.100	74.2122	246.269	12
	LS	100	1.944	1.957	1.946	1.949	33.7726	107.5754	12
Fe(qsal-I)$_2$·CH_2Cl_2	HS	298	2.103	2.130	2.007	2.080	65.0342	219.4995	12
	LS	100	1.938	1.949	1.955	1.947	40.8155	110.6237	12
Fe(qsal-F)$_2$	HS	123	2.170	2.187	2.016	2.124	86.6926	315.3685	12
[Fe(*t*Bu$_2$qsal)$_2$	HS	230	2.131	2.203	1.998	2.110	80.1754	287.5651	13
	LS	100	1.932	1.965	1.945	1.947	35.6014	117.7115	13
Fe(qsal-5NO_2)$_2$	LS	100	1.932	1.944	1.943	1.940	36.7217	110.4249	[14]
Fe(qsal-NEt_2)$_2$	HS	200	2.128	2.231	2.019	2.126	80.6957	273.0671	This work
	mixture	90	2.074	2.182	1.920	2.059	66.3037	235.5972	This work

[5] R. Ketkaew, Y. Tantirungrotechai, P. Harding, G. Chastanet, P. Guionneau, M. Marchivie and D. J. Harding, *Dalton Trans.*, 2021, **50(**3), 1086-1096.

[6] K. Sugimoto, T. Okubo, M. Maekawa and T. Kuroda-Sowa, *Cryst. Growth Des.*, 2021, **21(**7), 4178-4183.

[7] T. Kuroda-Sowa, K. Kimura, J. Kawasaki, T. Okubo and M. Maekawa, *Polyhedron*, 2011, **30(**18), 3189-3192.

[8] T. Kuroda-Sowa, Z. Yu, Y. Senzaki, K. Sugimoto, M. Maekawa, M. Munakata, S. Hayami and Y. Maeda, *Chem. Lett.*, 2008, **37(**12), 1216-1217.

[9] Z. Yu, T. Kuroda-Sowa, H. Kume, T. Okubo, M. Maekawa and M. Munakata, *Bull. Chem. Soc. Jpn.*, 2009, **82(**3), 333-337.

[10] T. Kuroda-Sowa, R. Isobe, N. Yamao, T. Fukumasu, T. Okubo and M. Maekawa, *Polyhedron*, 2017, **136**,74-78.

[11] W. Phonsri, C. G. Davies, G. N. L. Jameson, B. Moubaraki, J. S. Ward, P. E. Kruger, G. Chastanet and K. S. Murray, *Chem. Commun.*, 2017, **53(**8), 1374-1377.

[12] W. Phonsri, D. S. Macedo, K. R. Vignesh, G. Rajaraman, C. G. Davies, G. N. L. Jameson, B. Moubaraki, J. S. Ward, P. E. Kruger, G. Chastanet and K. S. Murray, *Chem. Eur. J.*, 2017, **23(**29), 7052-7065.

[13] M. Gakiya-Teruya, X. Jiang, D. Le, Ö. Üngör, A. J. Durrani, J. J. Koptur-Palenchar, J. Jiang, T. Jiang, M. W. Meisel, H.-P. Cheng, X.-G. Zhang, X.-X. Zhang, T. S. Rahman, A. F. Hebard and M. Shatruk, *J. Am. Chem. Soc.*, 2021, **143(**36), 14563-14572.

[14] O. Iasco, E. Rivière, R. Guillot, M. Buron-Le Cointe, J.-F. Meunier, A. Bousseksou and M.-L. Boillot, *Inorg. Chem.*, 2015, **54(**4), 1791-1799.

X-ray Powder diffraction diagram

PXRD was performed on a BRUKER APEX III c7 Diffractometer with a sample in capillary, a collimated microfocus source Cu Kα radiation (1.54178 Å) operating at 50kV / 1 mA. An Oxford Cryosystem 700 Plus low temperature Device was used to maintained the sample at 200K temperature. We prepared in the gloves box a glass capillary made of borosilicate glass with a diameter of 0.5 mm and sealed with vacuum grease. Data were processed using DIFFRAC.EVA (Version 3.2, Bruker AXS 2010-2013).

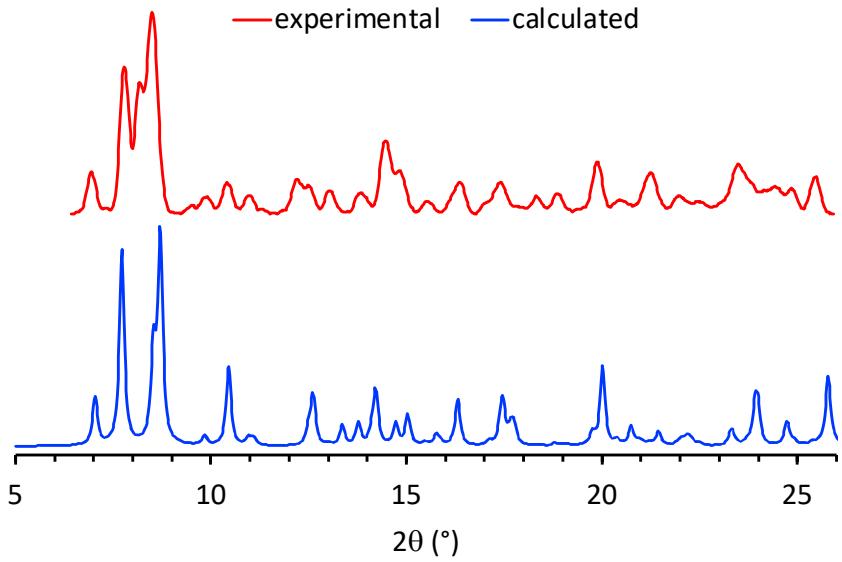

Figure S6. PXRD diagram of the microcrystalline powder of $[Fe(qsal\text{-}NEt_2)_2]\bullet 1.5MeOH$ (red trace) and calculated from the single crystal crystallographic structure (blue trace)

X-Ray Absorption Spectroscopy

Linear combination and determination of the reference spectra used:

Using linear combination, the proportions of molecules with Fe(III) and Fe(II) centers, as well as the proportions of Fe(II) molecules in high spin and low spin states, can be determined as:

$$XAS\ signal\ =\ a * XAS\ Fe(II)_{HS}\ +\ b * XAS\ Fe(II)_{LS}\ +\ c * XAS\ Fe(III)$$

where XAS signal is the experimental spectrum, a, b, and c are the proportions of Fe(II) molecules in the HS state, Fe(II) molecules in the LS state, and Fe(III) molecules respectively. XAS Fe(II) HS, XAS Fe(II) LS, and XAS Fe(III) are the reference spectrum for Fe(II) molecules in the HS state, Fe(II) molecules in the LS state,and Fe(III) molecules respectively.

The three reference spectra used are presented in Figure S8. To obtain the reference spectrum of Fe(III) molecules, we measured a powder of $[Fe^{III}(qsal\text{-}NEt_2)_2]Cl$. We observed that the spectra do not evolve with temperature, the Fe(III) derivative remains in high spin state at low temperature (Figure S8a). For the Fe(II) molecules in HS state, we observed that the submonolayer did not contain any Fe(III) molecules as discussed in the text. So, we used as a reference spectrum for Fe(II) molecules in HS the average over 5 curves recorded on a molecular film on graphene at 300 K. The LS reference spectrum was calculated from bulk measurements at 350 K and 100 K. All the reference spectra have been normalized to their integral value to be comparable. For the $Fe(qsal\text{-}NEt_2)_2$ submonolayer on gr/SiO_2, a shift of the signal arising from the low spin state is observed. Thus, for the linear combination on the submonolayer, the reference spectrum for the Fe(II) molecules in the LS state was shifted by -0.3 eV (see main text for calculations).

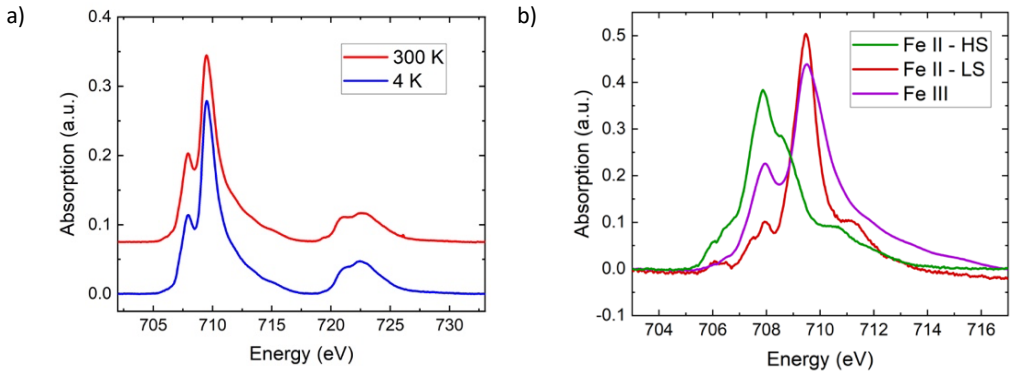

Figure S7. (a) Reference spectra at the Fe $L_{2,3}$ edges of the Fe(III) complex at T = 300 K and 4 K and (b) reference spectra at the Fe L_3-edge for Fe(II) complex in the HS state (green curve), in the LS state (red curve) and the Fe(III) complex (purple curve), used for all the linear combination to determine the proportion of each species.

Fitting of the spectra for the bulk material

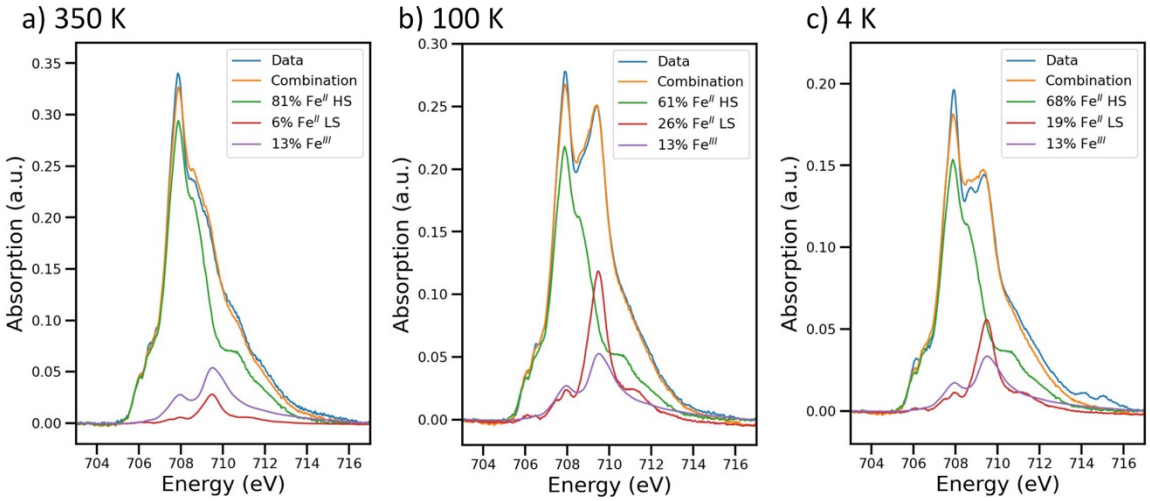

Figure S8. Fits of the Fe L_3-edge spectra for the powder of Fe(qsal-NEt_2)$_2$ at 350 K, 100 K, and 4 K. The experimental spectra are in blue, the linear combination in orange with the contribution of each reference spectra for the Fe(II) molecules in the high spin state (green curve), the Fe(II) molecules in the low spin state (red curve) and the Fe(III) molecules (purple curve).

Evolution under X-ray of the signal at 4 K for the bulk:

At 4 K, the absorption signal evolves with the exposure time to the X-ray. As can be observed in Figure S10, the signal at 709.3 eV is decreasing implying a decrease in the number of Fe(II) molecules in the low spin state. This is typical of the soft X-ray induced excited spin-state trapping (SOXIESST) effect for which the X-ray induces a LS-to-HS conversion. Quantitatively, for the first spectrum (0 minutes) the proportion of Fe(II) molecules in high spin state is 78±2%, and it increased to 85±2% after 3 minutes.

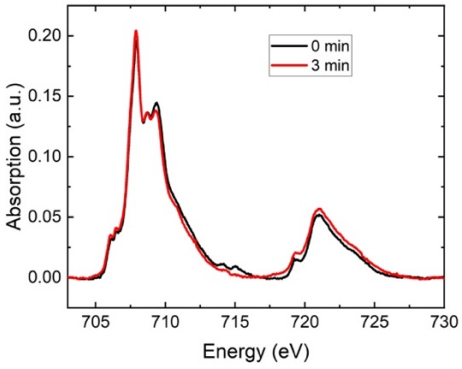

Figure S9. Evolution with time of the spectra recorded at the Fe $L_{2,3}$ edges acquired at 4K on the bulk microcrystalline powder.

Coverage calibration of the submonolayer:

Unfortunately, the system Fe(qsal-NEt_2)$_2$/graphene/SiO_2 is difficult to image and no STM calibration could be realized. To estimate the coverage, we used the calibration realized for Fe$(MPz)_2$ molecules on Au(111) for which a clear calibration between the relative Fe L_3 edge jump and the coverage determined by STM has been established.[15] In this case, the Fe$(MPz)_2$ molecules are arranged in a dense molecular layer, leading to a relative edge jump on Au(111) of 1.1%, for an iron density of 0.48 ± 0.06 Fe atom/nm^2.

Fe(qsal-NEt_2)$_2$/graphene/SiO_2 samples have been measured during the same beamtime as Fe$(MPz)_2$ on Au(111), for which the coverage can be directly determined using the previous calibration. Then by comparing the absolute Fe L_3 jumps of both samples, by measuring directly the current recorded on the electrometer, we have been able to estimate the coverage of Fe(qsal-NEt_2)$_2$ molecules on graphene/SiO_2. We thus estimated a density of 0.5 ± 0.2 molecule/nm^2. Not knowing if the molecules are arranged in a dense network or are randomly adsorbed, we prefer to give the coverage in terms of density. Nonetheless, this density can be compared to the one expected in dense planes of the molecular structure. The denser plane of the crystal is the (101) plane, in which the area of a unit cell is 1.2 nm^2 corresponding to a density of 0.9 molecule/nm^2. So, if the molecules on the graphene/SiO_2 are arranged as in this dense plane, the coverage would be 0.6 ML. If the molecules are randomly adsorbed, the density is such that isolated molecules can also be expected.

Fitting of the spectra for the submonolayer

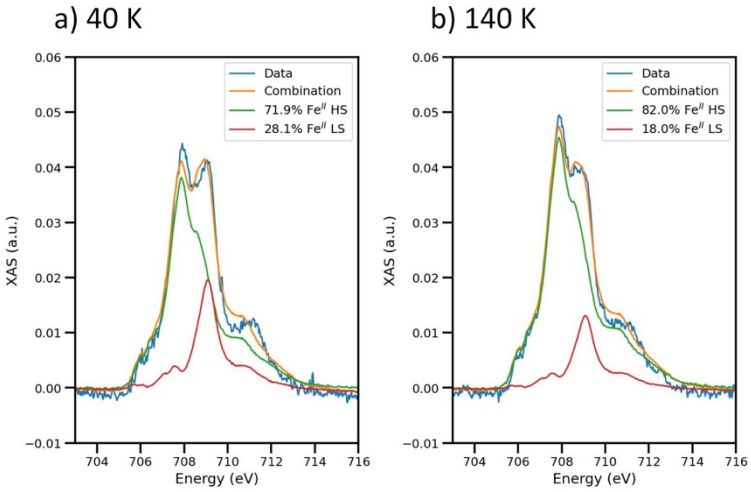

Figure S10. Fits of the Fe L_3-edge spectra for the Fe(qsal-NEt_2)$_2$ submonolayer on graphene at a) 40 K and b) 140 K. The experimental spectra are in blue, the linear combination in orange with the contribution of each reference spectra for the Fe(II) molecules in the high spin (green curve) and low spin (red curve) states.

[15] K. Bairagi, A. Bellec, C. Fourmental, O. Iasco, J. Lagoute, C. Chacon, Y. Girard, S. Rousset, F. Choueikani, E. Otero, P. Ohresser, P. Sainctavit, M. L. Boillot, T. Mallah and V. Repain, *J. Phys. Chem. C*, 2018, **122(**1), 29080-29080.

DFT Calculations

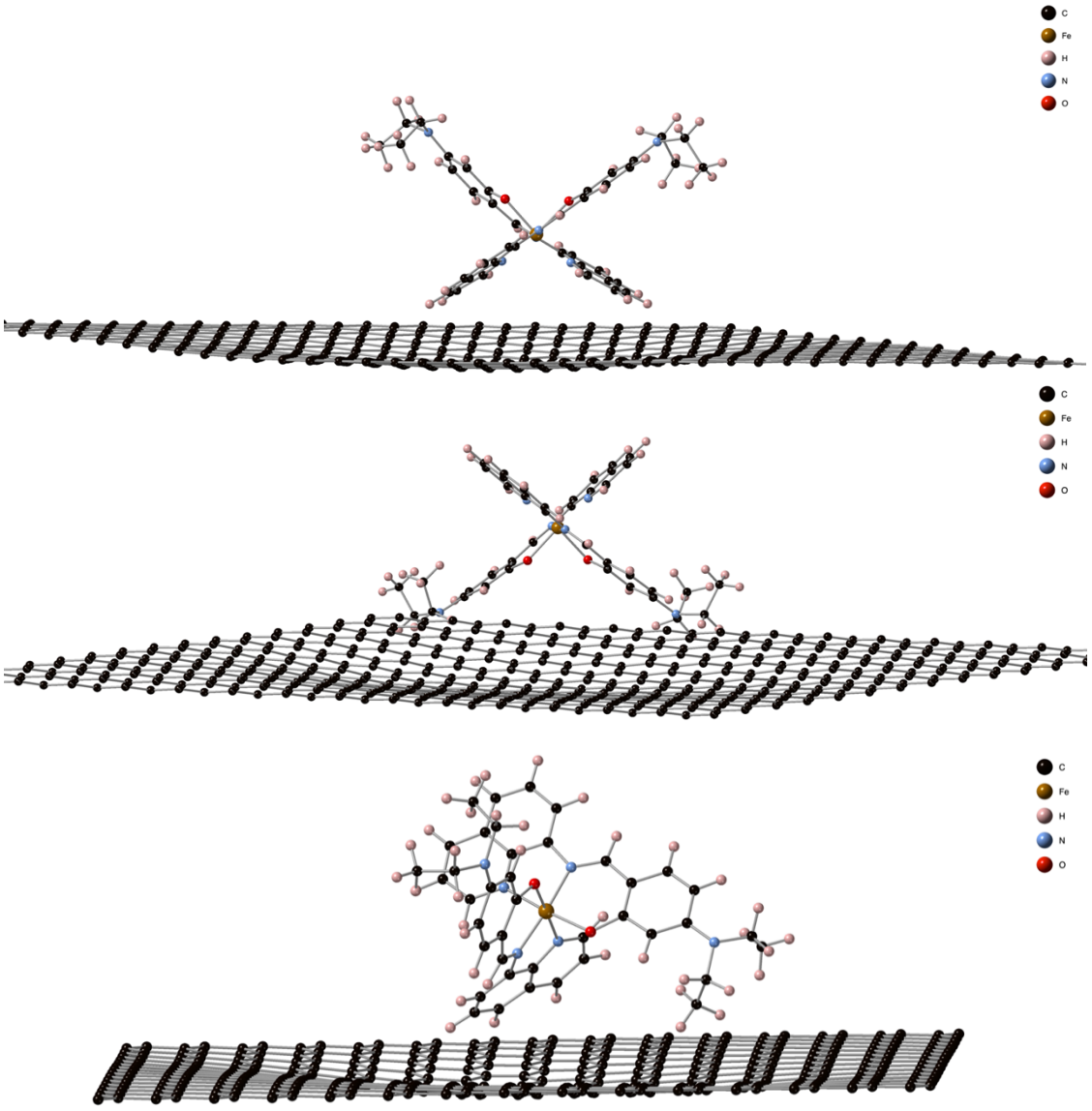

Figure S11. View the adsorption modes on graphene of the configurations cf1 (top), cf2 (middle) and cf3 (bottom)

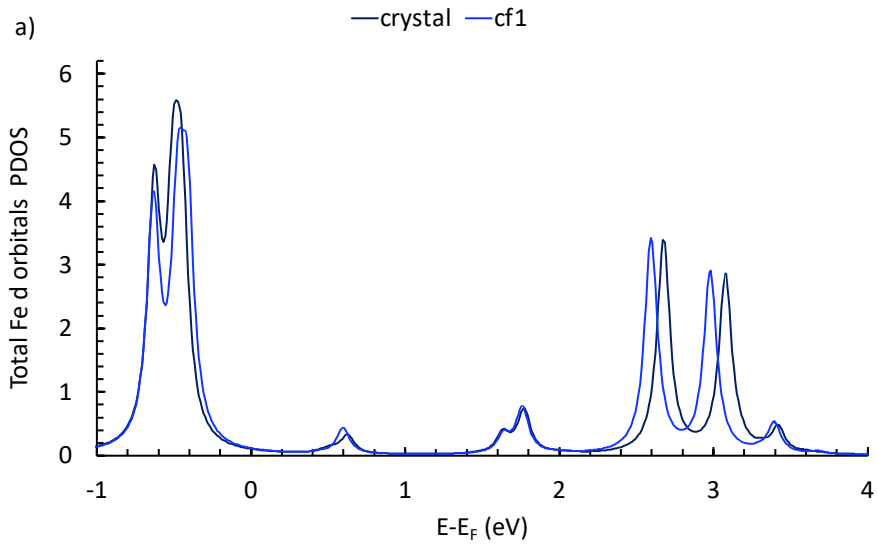

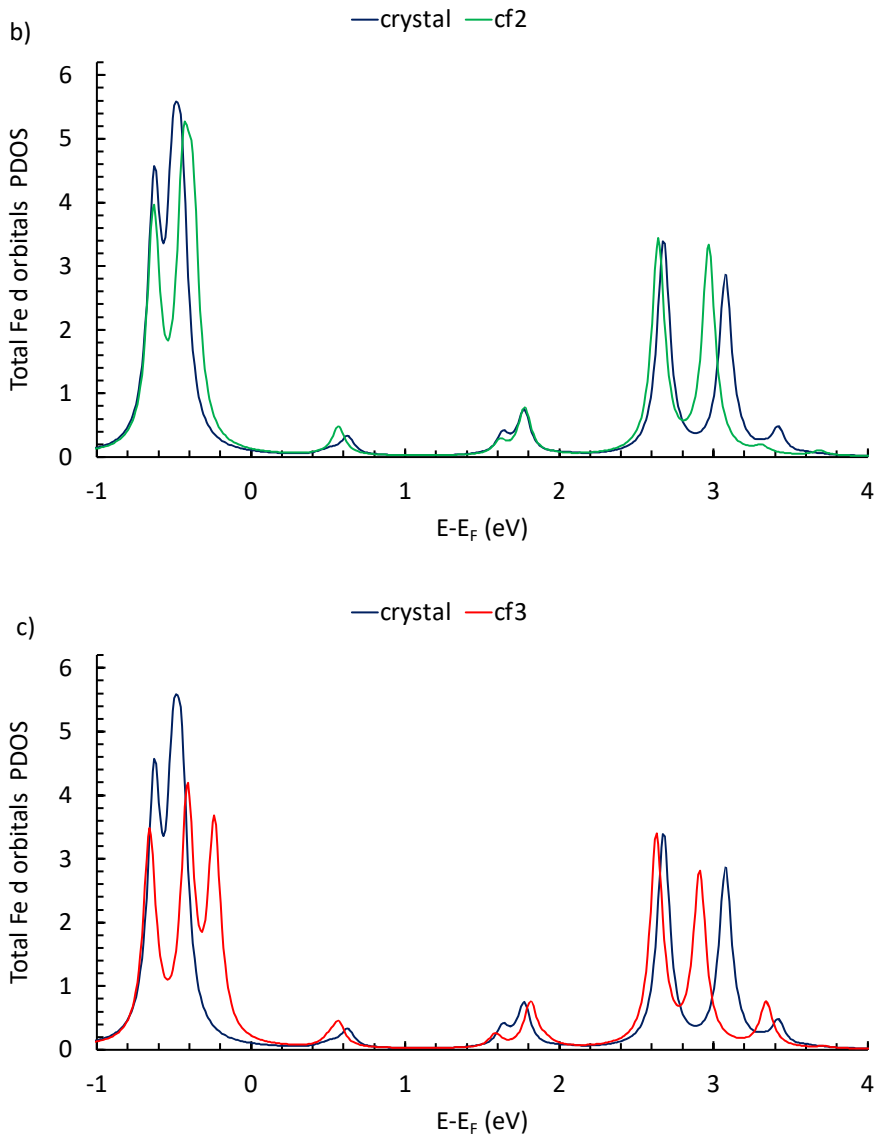

Figure S12. Total density of states of Fe atoms projected on the d orbitals for the molecule in the crystal and for the three configurations cf1 (a), cf2 (b) and cf3 (c).